

# Second quantization approach to COVID-19 epidemic

Leonardo Mondaini<sup>1</sup>, Bernhard Meirose<sup>2</sup> and Felipe Mondaini<sup>3</sup>

<sup>1</sup> Department of Physics, Federal University of the State of Rio de Janeiro, Rio de Janeiro, Brazil

<sup>2</sup> Fysiska institutionen, Lunds universitet, Lund, Sweden

<sup>3</sup> Centro Federal de Educação Tecnológica Celso Suckow da Fonseca, CEFET-RJ/ Campus Petrópolis, 25.620-003, Petrópolis, Brazil

\*All authors contributed equally to this work.

E-mail:

mondaini@unirio.br,bernhard.meirose@hep.lu.se,felipe.mondaini@cefet-rj.br

April 2021

**Abstract.** We show how the standard field theoretical language based on creation and annihilation operators may be used for a straightforward derivation of an SIR-type stochastic model for COVID-19 epidemic, from which we obtain the time evolution of the mean number of infectious (active cases) and deceased individuals. In order to capture the effects of lockdown and social distancing, we use a time-dependent infection rate. The results are in good agreement with the data for three different waves of epidemic activity in South Korea.

*Keywords:* Second Quantization, COVID-19 Epidemic, Stochastic Epidemic Models

## 1. Introduction

The year 2020 will be remembered in history as the year in which humanity suffered from the rapid spread of coronavirus disease 2019 (COVID-19), caused by the severe acute respiratory syndrome coronavirus 2 (SARS-CoV-2) and responsible for the worst pandemic in the last hundred years. Governments around the world were strongly impacted by the pandemic and, in addition to efforts of a social and economic nature, it became evident the need to bring together members of the international scientific community to analyze data on the evolution of the disease and propose concrete actions for the control and mitigation of its serious effects [1]. In this sense, even researchers from areas far from epidemiology were encouraged to collaborate with their experience and specific knowledge in the study of possible models for describing the evolution of the pandemic in different countries of the world [2, 3, 4, 5, 6], often serving as guides

for the actions of local governments. Theoretical particle physicists are used to dealing with problems and proposing models to describe complex phenomena involving the fundamental constituents of matter. In this work, we show how the usual field theoretical language based on creation and annihilation operators, usually used in the construction of these elementary particle models, may also be adapted to the construction of an epidemiological model for COVID-19 which can be compared to the data available for several countries. We believe this can serve as an stimulus so that other researchers working on these subjects can also contribute to this great scientific network.

In a pioneering work [7] it was shown that creation and annihilation operators (building blocks of the second quantization method and standard field theoretical language) are not limited to quantum systems and, in fact, may be introduced to the description of certain classical many-particle systems. Since then, this Fock space formalism (or field theoretical language) for classical systems was complemented by a path integral version and applied to the description of stochastic (birth-death) processes on lattices [8, 9] and tumour growth [10].

In what follows we show how this standard field theoretical language based on creation and annihilation operators may be used for a straightforward derivation of an SIR-type stochastic model for COVID-19 epidemic, from which we obtain the time evolution of the mean number of infectious (active cases) and deceased individuals in South Korea. Indeed, our main motivation comes from the fact that, as remarked in [11], for the types of models studied in population biology and epidemiology, this field theoretical description is notationally neater and more manageable than standard methods, often replacing sets of equations by single equations with the same content. As an example of this, we may stress that a single Hamiltonian function sums up the system dynamics compactly and may be easily written down from a verbal description of the transitions presented in our model. Besides the simplicity and notational appeal, we may stress as another advantage of our SIR-type model the use of a time-dependent infection rate in order to capture the effects of a lockdown, since the standard SIR model does not take these into account.

The rest of this work is organized as follows. In Section 2, we introduce the basic aspects of our model which allow us to obtain differential equations describing the time evolution of the mean number of infectious and deceased individuals, while the time-dependent infection rate used for data comparison is presented in Section 3. The differential equations are used to fit available data (South Korea) for the time evolution of infectious (active cases) individuals in Section 4 and deceased individuals in Section 5. Further data comparisons for two other distinct waves of epidemic activity in South Korea are presented in Section 6. Our conclusions are presented in Section 7.

## **2. Building the model**

We start by considering interacting populations, whose total sizes are allowed to change, composed of four types of individuals: susceptible, infectious, recovered and deceased.

Let us introduce  $\mathcal{S}(t)$ ,  $\mathcal{I}(t)$ ,  $\mathcal{R}(t)$  and  $\mathcal{D}(t)$  as random variables which represent, respectively, the number of susceptible, infectious, recovered and deceased individuals at a given time instant  $t$ .

We then consider a multivariate process  $\{(\mathcal{S}(t); \mathcal{I}(t); \mathcal{R}(t); \mathcal{D}(t))\}_{t=0}^{\infty}$  with a joint probability function given by

$$p_{(n_S, n_I, n_R, n_D)}(t) = \text{Prob}\{\mathcal{S}(t) = n_S; \mathcal{I}(t) = n_I; \mathcal{R}(t) = n_R; \mathcal{D}(t) = n_D\} . \quad (1)$$

Our aim is to compute time-dependent expectation values of the observables  $\mathcal{S}(t)$ ,  $\mathcal{I}(t)$ ,  $\mathcal{R}(t)$  and  $\mathcal{D}(t)$ , which may be defined in terms of the configuration probability according to

$$\begin{aligned} \langle \mathcal{S}(t) \rangle &= \sum_{n_S, n_I, n_R, n_D} n_S p_{(n_S, n_I, n_R, n_D)}(t) ; \\ \langle \mathcal{I}(t) \rangle &= \sum_{n_S, n_I, n_R, n_D} n_I p_{(n_S, n_I, n_R, n_D)}(t) ; \\ \langle \mathcal{R}(t) \rangle &= \sum_{n_S, n_I, n_R, n_D} n_R p_{(n_S, n_I, n_R, n_D)}(t) ; \\ \langle \mathcal{D}(t) \rangle &= \sum_{n_S, n_I, n_R, n_D} n_D p_{(n_S, n_I, n_R, n_D)}(t) . \end{aligned} \quad (2)$$

The probabilistic state of the system may be represented by the vector

$$|\nu_S, \nu_I, \nu_R, \nu_D\rangle_t = \sum_{n_S, n_I, n_R, n_D} p_{(n_S, n_I, n_R, n_D)}(t) |n_S, n_I, n_R, n_D\rangle , \quad (3)$$

with the normalization condition  $\sum_{n_S, n_I, n_R, n_D} p_{(n_S, n_I, n_R, n_D)}(t) = 1$ .

Since the configurations are given entirely in terms of occupation numbers  $(n_S, n_I, n_R, n_D)$ , which calls for a representation in terms of second-quantized bosonic operators [9], we introduce *creation* and *annihilation* operators for the susceptible, infectious, recovered and deceased individuals, respectively,  $a_S$  and  $a_S^\dagger$ ,  $a_I$  and  $a_I^\dagger$ ,  $a_R$  and  $a_R^\dagger$ ,  $a_D$  and  $a_D^\dagger$ .

These operators must satisfy the following commutation relations

$$\begin{aligned} [a_i, a_j^\dagger] &= \delta_{ij} ; \\ [a_i, a_j] &= [a_i^\dagger, a_j^\dagger] = 0 , \end{aligned} \quad (4)$$

where  $i, j = \{S, I, R, D\}$  and  $\delta_{ij}$  is the Kronecker delta ( $\delta_{ij} = 1$  if  $i = j$  and  $\delta_{ij} = 0$  if  $i \neq j$ ). As usual in the second quantization framework, we say

that  $a_S^\dagger$ ,  $a_I^\dagger$ ,  $a_R^\dagger$  and  $a_D^\dagger$  “create” , respectively, susceptible, infectious, recovered and deceased individuals when applied over the reference (vacuum) state  $|0, 0, 0, 0\rangle$ . This allows us to build our space from basis vectors of the form  $|n_S, n_I, n_R, n_D\rangle = \left(a_S^\dagger\right)^{n_S} \left(a_I^\dagger\right)^{n_I} \left(a_R^\dagger\right)^{n_R} \left(a_D^\dagger\right)^{n_D} |0, 0, 0, 0\rangle$ .

This vacuum state has the following properties:  $a_S |0, 0, 0, 0\rangle = a_I |0, 0, 0, 0\rangle = a_R |0, 0, 0, 0\rangle = a_D |0, 0, 0, 0\rangle = 0$  (from which “annihilation” operators) and  $\langle 0, 0, 0, 0 | 0, 0, 0, 0\rangle = 1$  (inner product).

Following the above definitions, we also have

$$\begin{aligned}
 a_S^\dagger |n_S, n_I, n_R, n_D\rangle &= |n_S + 1, n_I, n_R, n_D\rangle ; \\
 a_I^\dagger |n_S, n_I, n_R, n_D\rangle &= |n_S, n_I + 1, n_R, n_D\rangle ; \\
 a_R^\dagger |n_S, n_I, n_R, n_D\rangle &= |n_S, n_I, n_R + 1, n_D\rangle ; \\
 a_D^\dagger |n_S, n_I, n_R, n_D\rangle &= |n_S, n_I, n_R, n_D + 1\rangle ; \\
 a_S |n_S, n_I, n_R, n_D\rangle &= n_S |n_S - 1, n_I, n_R, n_D\rangle ; \\
 a_I |n_S, n_I, n_R, n_D\rangle &= n_I |n_S, n_I - 1, n_R, n_D\rangle ; \\
 a_R |n_S, n_I, n_R, n_D\rangle &= n_R |n_S, n_I, n_R - 1, n_D\rangle ; \\
 a_D |n_S, n_I, n_R, n_D\rangle &= n_D |n_S, n_I, n_R, n_D - 1\rangle .
 \end{aligned} \tag{5}$$

Since

$$\begin{aligned}
 a_S^\dagger a_S |n_S, n_I, n_R, n_D\rangle &= n_S |n_S, n_I, n_R, n_D\rangle ; \\
 a_I^\dagger a_I |n_S, n_I, n_R, n_D\rangle &= n_I |n_S, n_I, n_R, n_D\rangle ; \\
 a_R^\dagger a_R |n_S, n_I, n_R, n_D\rangle &= n_R |n_S, n_I, n_R, n_D\rangle ; \\
 a_D^\dagger a_D |n_S, n_I, n_R, n_D\rangle &= n_D |n_S, n_I, n_R, n_D\rangle ,
 \end{aligned} \tag{6}$$

we may conclude that the operators  $n_S = a_S^\dagger a_S$ ,  $n_I = a_I^\dagger a_I$ ,  $n_R = a_R^\dagger a_R$  and  $n_D = a_D^\dagger a_D$  just count the number of individuals in a definite state, reason why they are called *number operators*. Note that the vector state of our system may be then rewritten in terms of creation and annihilation operators as

$$\begin{aligned}
 |\nu_S, \nu_I, \nu_R, \nu_D\rangle_t &= \sum_{n_S, n_I, n_R, n_D} p_{(n_S, n_I, n_R, n_D)}(t) \\
 &\times \left(a_S^\dagger\right)^{n_S} \left(a_I^\dagger\right)^{n_I} \left(a_R^\dagger\right)^{n_R} \left(a_D^\dagger\right)^{n_D} |0, 0, 0, 0\rangle .
 \end{aligned} \tag{7}$$

The time evolution of our system will then be generated by a linear operator  $\mathcal{H}$  (*Hamiltonian*) which may be constructed directly from the the transition rates present

**Table 1.** Transition rates presented in our model and corresponding terms in the Hamiltonian  $\mathcal{H}$ .

Transition	Description	Contribution to $\mathcal{H}$
$\mathcal{S} \xrightarrow{\beta} \mathcal{I}$	infection (rate $\beta$ )	$\beta(a_S^\dagger a_S - a_I^\dagger a_S)$
$\mathcal{I} \xrightarrow{(1-\sigma)\gamma} \mathcal{R}$	change infectious $\rightarrow$ recovered (rate $(1-\sigma)\gamma$ )	$(1-\sigma)\gamma(a_I^\dagger a_I - a_R^\dagger a_I)$
$\mathcal{I} \xrightarrow{\sigma\gamma} \mathcal{D}$	change infectious $\rightarrow$ deceased (rate $\sigma\gamma$ )	$\sigma\gamma(a_I^\dagger a_I - a_D^\dagger a_I)$

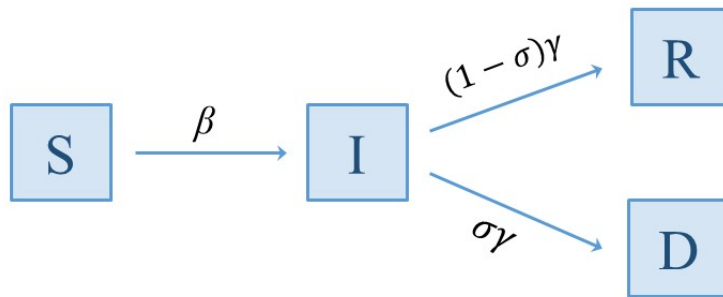


**Figure 1.** The structure of our SIR-type model. The rate  $\beta$  is related to the infection rate of the virus and  $\gamma$  is related to the time required to infected people to become recovered or deceased. Both parameters have the dimension of  $\text{time}^{-1}$ . Indeed,  $\gamma = 1/D$ , where  $D$  is the average time period during which an individual remains infectious, before one gets recovered or deceased. The parameter  $\sigma$  (the case fatality rate) is dimensionless and represents the percentage of infected people who become deceased.

in our model according to Table 1 (cf. [11], Table 1). In Figure 1 we present a compartmental diagram for the structure of our SIR-type model.

Note that, upon summing up the terms presented in Table 1 and rearranging them, we may write down our Hamiltonian as

$$\mathcal{H} = \beta n_S + \gamma n_I - \left[ \beta a_I^\dagger a_S + (1-\sigma)\gamma a_R^\dagger a_I + \sigma\gamma a_D^\dagger a_I \right]. \quad (8)$$

The notational advantage of this field theoretical description is made clear at this point if we observe that, from the above definitions, the equation which represents the flux of probability between states at rates defined by our model (the so-called *master equation* or *forward Kolmogorov differential equation* [12]) takes the very compact form of an imaginary-time Schrödinger-type linear equation, namely

$$\frac{d}{dt} |\nu_S, \nu_I, \nu_R, \nu_D\rangle_t = -\mathcal{H} |\nu_S, \nu_I, \nu_R, \nu_D\rangle_t. \quad (9)$$

We can get, after some algebra, a more common representation for the master equation by substituting the expressions for the Hamiltonian, (8), and the vector state, (3), into (9)

$$\begin{aligned} \frac{d}{dt} p_{(n_S, n_I, n_R, n_D)}(t) = & -(\beta n_S + \gamma n_I) p_{(n_S, n_I, n_R, n_D)}(t) \\ & + \beta(n_S + 1) p_{(n_S+1, n_I-1, n_R, n_D)}(t) \\ & + (1 - \sigma)\gamma(n_I + 1) p_{(n_S, n_I+1, n_R-1, n_D)}(t) \\ & + \sigma\gamma(n_I + 1) p_{(n_S, n_I+1, n_R, n_D-1)}(t) . \end{aligned} \quad (10)$$

In order to compute the time-dependent expectation values of the observables  $\mathcal{S}(t)$ ,  $\mathcal{I}(t)$ ,  $\mathcal{R}(t)$  and  $\mathcal{D}(t)$  through the above master equation, we follow the well-established methodology presented in [12] and introduce the following *moment generating function (mgf)*

$$\begin{aligned} M(\phi_S, \phi_I, \phi_R, \phi_D; t) &= \langle e^{\phi_S \mathcal{S}(t)} e^{\phi_I \mathcal{I}(t)} e^{\phi_R \mathcal{R}(t)} e^{\phi_D \mathcal{D}(t)} \rangle \\ &= \sum_{n_S, n_I, n_R, n_D} p_{(n_S, n_I, n_R, n_D)}(t) e^{n_S \phi_S + n_I \phi_I + n_R \phi_R + n_D \phi_D} . \end{aligned} \quad (11)$$

Note that from the above equation we have

$$\begin{aligned} \left[ \frac{\partial M}{\partial \phi_S} \right]_{\phi_S, \phi_I, \phi_R, \phi_D=0} &= \sum_{n_S, n_I, n_R, n_D} n_S p_{(n_S, n_I, n_R, n_D)}(t) = \langle \mathcal{S}(t) \rangle ; \\ \left[ \frac{\partial M}{\partial \phi_I} \right]_{\phi_S, \phi_I, \phi_R, \phi_D=0} &= \sum_{n_S, n_I, n_R, n_D} n_I p_{(n_S, n_I, n_R, n_D)}(t) = \langle \mathcal{I}(t) \rangle ; \\ \left[ \frac{\partial M}{\partial \phi_R} \right]_{\phi_S, \phi_I, \phi_R, \phi_D=0} &= \sum_{n_S, n_I, n_R, n_D} n_R p_{(n_S, n_I, n_R, n_D)}(t) = \langle \mathcal{R}(t) \rangle ; \\ \left[ \frac{\partial M}{\partial \phi_D} \right]_{\phi_S, \phi_I, \phi_R, \phi_D=0} &= \sum_{n_S, n_I, n_R, n_D} n_D p_{(n_S, n_I, n_R, n_D)}(t) = \langle \mathcal{D}(t) \rangle . \end{aligned} \quad (12)$$

Multiplying (10) by  $\exp(n_S \phi_S + n_I \phi_I + n_R \phi_R + n_D \phi_D)$  and summing on  $(n_S, n_I, n_R, n_D)$ , leads, after some algebra, to

$$\frac{\partial M}{\partial t} = [\beta (e^{-\phi_S + \phi_I} - 1)] \frac{\partial M}{\partial \phi_S} + [\gamma (e^{-\phi_I + \phi_R} - 1) + \sigma\gamma (e^{-\phi_I + \phi_D} - e^{-\phi_I + \phi_R})] \frac{\partial M}{\partial \phi_I} . \quad (13)$$

Hence, by differentiating the above equation with respect to  $\phi_S, \phi_I, \phi_R, \phi_D$  and evaluating the result at  $\phi_S, \phi_I, \phi_R, \phi_D = 0$  we get the following differential equations for  $\langle \mathcal{S}(t) \rangle$ ,  $\langle \mathcal{I}(t) \rangle$ ,  $\langle \mathcal{R}(t) \rangle$  and  $\langle \mathcal{D}(t) \rangle$ :

$$\begin{aligned}
\left[ \frac{\partial^2 M}{\partial t \partial \phi_S} \right]_{\phi_S, \phi_I, \phi_R, \phi_D=0} &= \frac{d}{dt} \langle \mathcal{S}(t) \rangle = -\beta \langle \mathcal{S}(t) \rangle ; \\
\left[ \frac{\partial^2 M}{\partial t \partial \phi_I} \right]_{\phi_S, \phi_I, \phi_R, \phi_D=0} &= \frac{d}{dt} \langle \mathcal{I}(t) \rangle = \beta \langle \mathcal{S}(t) \rangle - \gamma \langle \mathcal{I}(t) \rangle ; \\
\left[ \frac{\partial^2 M}{\partial t \partial \phi_R} \right]_{\phi_S, \phi_I, \phi_R, \phi_D=0} &= \frac{d}{dt} \langle \mathcal{R}(t) \rangle = (1 - \sigma) \gamma \langle \mathcal{I}(t) \rangle ; \\
\left[ \frac{\partial^2 M}{\partial t \partial \phi_D} \right]_{\phi_S, \phi_I, \phi_R, \phi_D=0} &= \frac{d}{dt} \langle \mathcal{D}(t) \rangle = \sigma \gamma \langle \mathcal{I}(t) \rangle .
\end{aligned} \tag{14}$$

Last but not least, we must observe at this point that the above differential equations would be the same if we have considered time-dependent rates  $(\beta(t), \gamma(t))$  from the very beginning. This turns out to be an important aspect of our model as we shall see in the next section.

### 3. Comparison to COVID-19 Epidemic Data - South Korea

We now compare our model against public epidemic data from South Korea, which was taken from the ‘‘Worldometer’’ reference website [13]. The modeled data for the number of deaths and number of active cases was compared to the data reported in South Korea during 96 days of the epidemic. In order to take into account the slowdown of the spread due the effects of quarantine and social distancing we use a similar approach to [14], where the infection rate  $\beta$  is a function of time ( $\beta \equiv \beta(t)$ ). Specifically,  $\beta(t) = \beta_0$  before a time  $t_{th}$ , while it exponentially decays for  $t > t_{th}$ . In our approach, however, we treat the period prior to lockdown and social actions with a a linearly growing  $\beta(t)$  function, instead of a constant, i.e.:

$$\beta(t) = \beta_0 t \quad \text{for } 0 \leq t < t_{th} , \tag{15}$$

and due to function continuity the expression for  $\beta(t)$  after lockdown measures becomes:

$$\beta(t) = t_{th} \beta_0 e^{-(t-t_{th})/\tau} \quad \text{for } t \geq t_{th} , \tag{16}$$

where the time  $t_{th}$  represents the starting time of the quarantine actions, while  $\tau$  refers to the decaying period and it has the dimension of time.

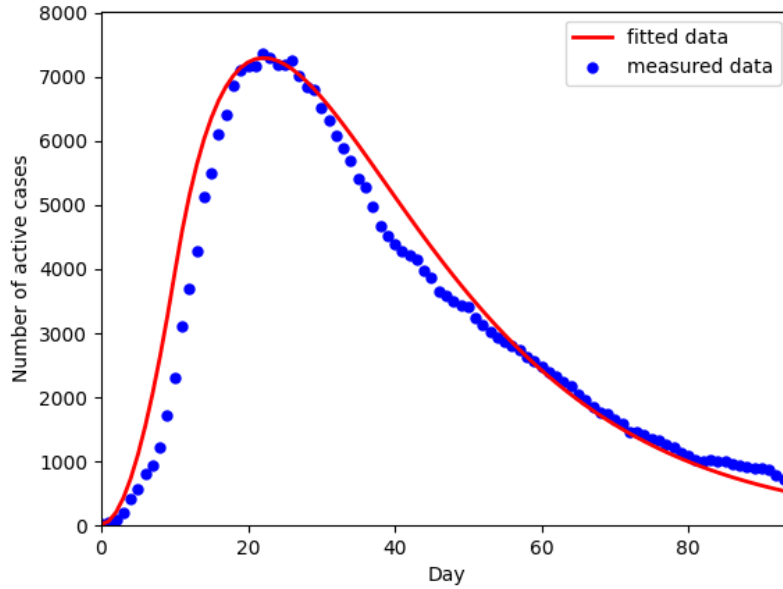


**Figure 2.** Number of active cases of COVID-19 in South Korea during 96 days of the epidemic corresponding to first wave of infections in the country. Modeled data is shown by the continuous red line, while measured data is depicted by the blue points.

#### 4. Number of active cases

For the number of active cases, we perform a weighted fit of the model allowing four of the five free parameters to vary (the number of active cases is independent of  $\sigma$ , the case fatality rate, discussed in Section 5) using least squares minimization with the LMFIT [15] package in Python 3.6.8. We use a population size of  $N = 5.164 \times 10^7$  people and as initial condition we use 19 active cases, the number of registered cases on the 18th of February in South Korea according to the Worldometer database. The end date of this first wave of infections is set to May 23, 2020.

The resulting fit, obtained by solving (14) for  $\langle \mathcal{I}(t) \rangle$ , overlaid with the real data points is shown in Figure 2. We also obtain the mean absolute percentage error ( $M$ ) of the real data and the fitted data points and achieve  $M = 14.7\%$ , which indicates acceptable agreement.

##### 4.1. Fitted parameters

The best fit is given by the following set of parameters:

$$\begin{aligned} \beta_0 &= 1.898 \times 10^{-6} \pm 1.202 \times 10^{-7} & , & & \gamma &= 0.0710 \pm 0.0127 & , \\ t_{th} &= 10.008 \pm 0.868 & , & & \tau &= 19.010 \pm 3.029 & , \end{aligned}$$

where the estimated uncertainties, calculated by LMFIT, are done by inverting the Hessian matrix, which represents the second derivative of fit quality for each variable parameter. It is interesting to note that  $1/\gamma$ , the time required to infected people to become recovered or deceased, is estimated to be  $1/0.017 \sim 14$  days. The uncertainty on this value is, however, large (18%), but even the shortest (12 days) and longest (17 days) values are within acceptable ranges for the average duration of the disease [16]. The  $\beta_0$  parameter, which is the initial constant for the infection rate, is a small number, which is unsurprising given that we have considered the infection rate to grow linearly with time until lockdown measures are in place. The value of  $t_{th}$  is interpreted as the day lockdown and social distancing measures started in South Korea during the first wave of infections.

## 5. Case fatality rate

The case fatality rate ( $\sigma$ ) in South Korea between February 18 and May 23, 2020 was obtained from the number of registered deaths. Figure 3 shows the modeled data (red), the solution for  $\langle \mathcal{D}(t) \rangle$  in (14), overlaid with the measured data (blue), and reasonable agreement can be seen between them. The best fit of the measured data to our model is given by:

$$\sigma = 0.0109 \pm 0.0011 ,$$

which corresponds to a rate of  $\sim 1.1\%$ .

## 6. Second and third outbreaks in South Korea

South Korea has experienced three waves of the COVID-19 pandemic, as can be seen on Figure 4, which shows the total number of active cases as a function of time (days) using data taken from the Worldometer reference website. As our model was able to reasonably model the first wave of infections, it is worth checking its explanatory power during the second and third COVID-19 waves for the same country. There is no strict definition for what an epidemic wave is, with the term simply implying natural pattern of peaks and valleys of contaminated individuals. Thus, we define the second wave between August 10, 2020 and October 1st 2020 and fit the data to our model using the same approach as for the first wave. The result for the second wave can be seen on Figure 5, with the best fit given by the following set of parameters:

$$\begin{aligned} \beta_0 &= 7.666 \times 10^{-7} \pm 2.086 \times 10^{-8} & , & & \gamma &= 0.0741 \pm 4.110 \times 10^{-5} , \\ t_{th} &= 15.653 \pm 0.388 & , & & \tau &= 12.589 \pm 0.643 . \end{aligned}$$

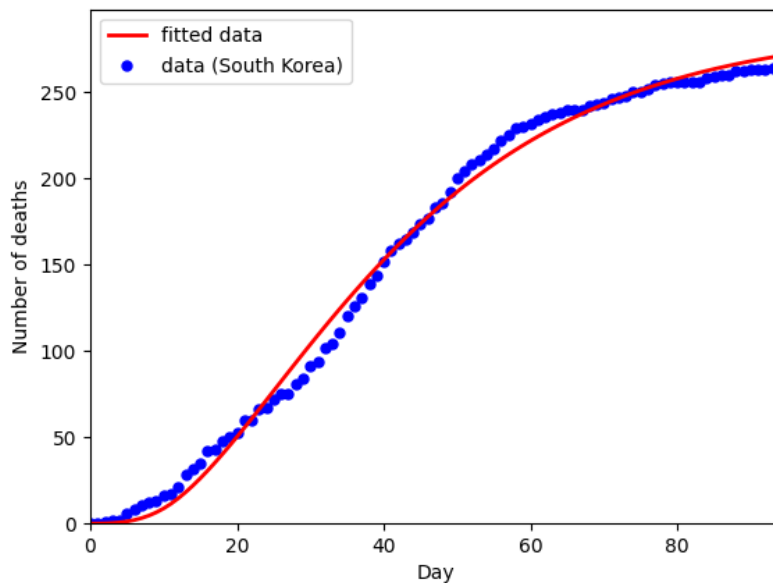


**Figure 3.** Number of deaths in South Korea during 96 days of the epidemic. Modeled data is shown by the continuous red line, while measured data is depicted by the blue points.

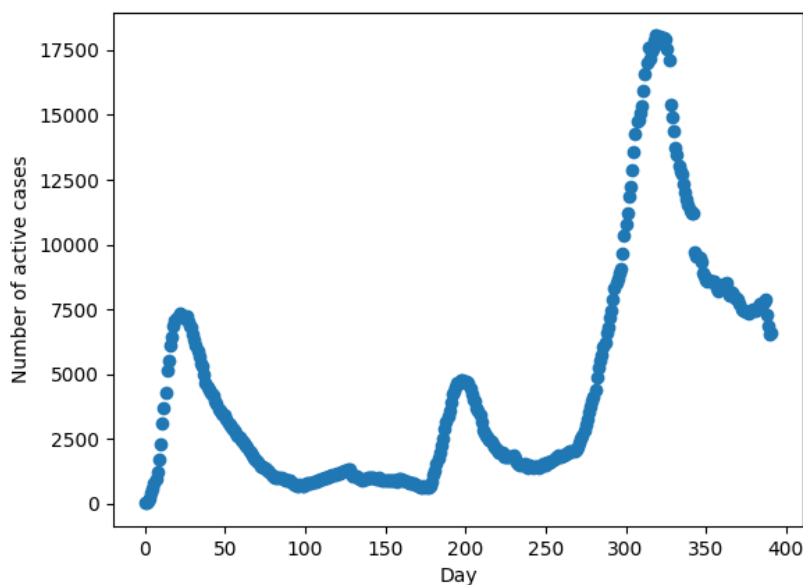


**Figure 4.** Number of active cases of COVID-19 in South Korea between February 18, 2020 and March 16, 2021. Three distinct waves of epidemic activity can be clearly seen from the above data.

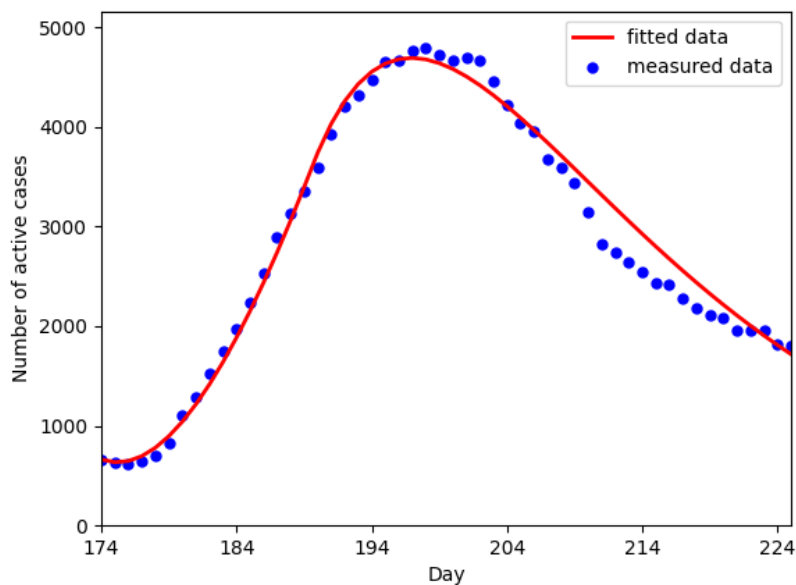


**Figure 5.** Number of active cases of COVID-19 in South Korea during 53 days of the epidemic corresponding to the so-called second wave of infections. Modeled data is shown by the continuous red line, while measured data is depicted by the blue points.

The mean absolute percentage error for the fit is of 5%, which points to an even better agreement compared to the first wave, a fact that is partially explained by the better available statistics. It must also be noted that the end of the second wave of infections quite rapidly became the start of the third wave, reason the data was truncated already on October 1st, i.e., 16 no longer holds, after around that date. The good agreement during the expanding phase, followed by a worse agreement during the decay phase seen in Figure 5 can be partially attributed to it.

Figure 6 shows the result for the third epidemic wave in South Korea, between November 06 2020 and February 06 2021. The  $\beta_0$  parameter is of the same order of magnitude as for the second wave and there is also similar agreement, with a mean absolute percentage error of 5.7%.

## 7. Concluding Remarks

We have investigated, using an SIR-type stochastic model for COVID-19 epidemic as a fundamental tool, the time evolution of the mean number of infectious (active cases) and deceased individuals in South Korea. Our model was able to describe the available data successfully. To the best of our knowledge, it is the first COVID-19 model built from standard field theoretical language. Despite its simplicity, the model was able to describe three waves of infections of the COVID-19 pandemic in South Korea, which shows its robustness and versatility. Studies including a non-susceptible subset of the population due to vaccinations and its effect on the infection rates, as well as comparisons with

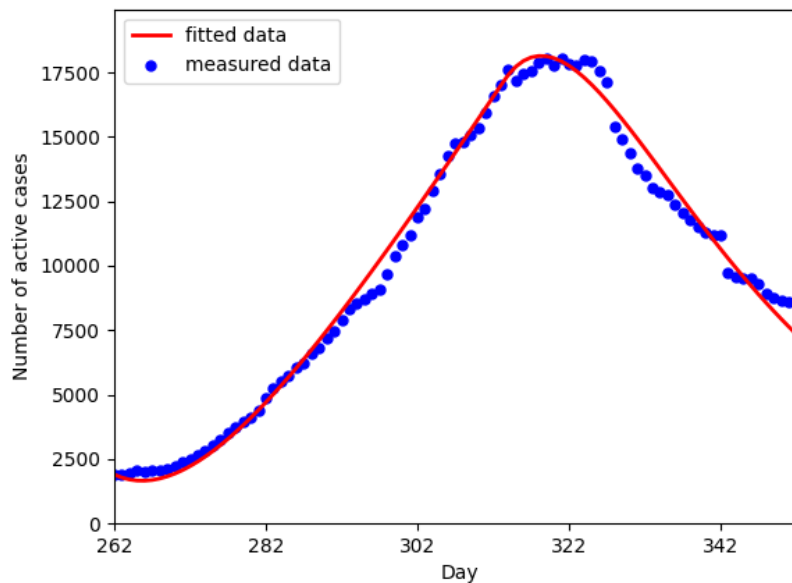


**Figure 6.** Number of active cases of COVID-19 in South Korea during 93 days of the epidemic corresponding to the so-called third wave of infections. Modeled data is shown by the continuous red line, while measured data is depicted by the blue points.

data from other countries are possible future directions to be explored with our model.

## References

- [1] Law K B, Peariasamy K M, Gill B S, Singh S, Sundram B M, Rajendran K, Dass S C, Lee Y L, Goh P P, Ibrahim H *et al.* 2020 *Scientific reports* **10** 1–11
- [2] Thomas D M, Sturdivant R, Dhurandhar N V, Debroy S and Clark N 2020 *Obesity* **28** 1375–1377
- [3] Zhuang Z, Zhao S, Lin Q, Cao P, Lou Y, Yang L, Yang S, He D and Xiao L 2020 *International Journal of Infectious Diseases* **95** 308–310
- [4] Zhao S, Lin Q, Ran J, Musa S S, Yang G, Wang W, Lou Y, Gao D, Yang L, He D *et al.* 2020 *International journal of infectious diseases* **92** 214–217
- [5] Neves A G and Guerrero G 2020 *Physica D: Nonlinear Phenomena* **413** 132693
- [6] Medo M 2020 *Journal of Physics A: Mathematical and Theoretical* **54** 035601
- [7] Doi M 1976 *Journal of Physics A: Mathematical and General* **9** 1465
- [8] Peliti L 1986 *Journal of Physics A: Mathematical and General* **19** L365
- [9] Cardy J L 1998 *Journal of Statistical Physics* **90** 1–56 ISSN 0022-4715 URL <http://dx.doi.org/10.1023/A:1023233431588>
- [10] Mondaini L 2017 *Journal of Applied Mathematics and Physics* **05** 1092–1098 ISSN 2327-4379 URL <http://dx.doi.org/10.4236/jamp.2017.55095>
- [11] Dodd P J and Ferguson N M 2009 *PloS one* **4** e6855
- [12] Allen L J 2010 *An introduction to stochastic processes with applications to biology* (CRC Press)
- [13] COVID-19 Coronavirus Pandemic data 2021 Worldometer [Online; accessed 24-March-2021] URL <https://www.worldometers.info/coronavirus/>

- [14] Palladino A, Nardelli V, Atzeni L G, Cantatore N, Cataldo M, Croccolo F, Estrada N and Tombolini A 2020 *arXiv preprint arXiv:2005.08724*
- [15] Newville M, Stensitzki T, Allen D B, Rawlik M, Ingargiola A and Nelson A 2016 *Astrophysics Source Code Library* ascl-1606
- [16] Fernández-Villaverde J and Jones C I 2020 Estimating and simulating a sird model of covid-19 for many countries, states, and cities Tech. rep. National Bureau of Economic Research